Naval Research Laboratory

Washington, DC 20375-5000

NRL Memorandum Report 6765

Observation of Harmonic Gyro-Backward-Wave Oscillation in a 100 GHz CARM Oscillator Experiment

ROBERT B. MCCOWAN, CAROL A. SULLIVAN,
STEVEN H. GOLD AND ARNE W. FLIFLET

Beam Physics Branch
Plasma Physics Division

February 16, 1991

REPORT DOCUMENTATION PAGE

Form Approved
OMB No. 0704-0188

1. AGENCY USE ONLY (Leave blank)	2. REPORT DATE	3. REPORT TYPE AND DATES COVERED
	1991 February 16	Interim

4. TITLE AND SUBTITLE
Observation of Harmonic Gyro-Backward-Wave Oscillation in a 100 GHz CARM Oscillator Experiment

5. FUNDING NUMBERS
ONR

J. O. #47-3046-0-1

6. AUTHOR(S)
Robert B. McCowan, Carol A. Sullivan, Steven H. Gold and Arne W. Fliflet

7. PERFORMING ORGANIZATION NAME(S) AND ADDRESS(ES)
NRL
Washington, DC 20375-5000

8. PERFORMING ORGANIZATION REPORT NUMBER
NRL Memorandum Report 6765

9. SPONSORING / MONITORING AGENCY NAME(S) AND ADDRESS(ES)
ONR
Arlington, VA 22217

10. SPONSORING / MONITORING AGENCY REPORT NUMBER

11. SUPPLEMENTARY NOTES

12a. DISTRIBUTION / AVAILABILITY STATEMENT
Approved for public release; distribution unlimited.

12b. DISTRIBUTION CODE

13. ABSTRACT *(Maximum 200 words)*

A cyclotron autoresonance maser (CARM) oscillator experiment is reported, using a 600 keV, 200 A electron beam, and a whispering-gallery-mode rippled-wall Bragg cavity. This device was designed to produce tens of megawatts of radiation at 100 GHz from a CARM interaction, but instead has produced only moderate powers (tens of kWs) in fundamental gyrotron modes near 35 GHz, in third-harmonic-gyro-BWO modes, and possible third-harmonic gyrotron modes at frequencies near the expected CARM frequency, with no discernable CARM radiation. The lack of observable CARM radiation is attributed to excessive ripple on the voltage waveform and to mode competition. Calculations of the spectrum and growth rate of the backward-wave oscillations are consistent with the experimental observation.

14. SUBJECT TERMS
CARM
Cyclotron-autoresonant-maser
High-power microwaves

15. NUMBER OF PAGES
22

16. PRICE CODE

17. SECURITY CLASSIFICATION OF REPORT	18. SECURITY CLASSIFICATION OF THIS PAGE	19. SECURITY CLASSIFICATION OF ABSTRACT	20. LIMITATION OF ABSTRACT
UNCLASSIFIED	UNCLASSIFIED	UNCLASSIFIED	SAR

NSN 7540-01-280-5500

Standard Form 298 (Rev 2-89)
Prescribed by ANSI Std Z39-18
298-102

CONTENTS

OBSERVATION OF HARMONIC GYRO-BACKWARD-WAVE OSCILLATION IN A 100 GHz CARM OSCILLATOR EXPERIMENT

I. Introduction

The cyclotron autoresonance maser (CARM) is a promising source of high-power radiation in the 100 GHz to 500 GHz frequency range that may have application in such areas as millimeter-wave radar and communications systems. The requirements for guide magnetic-field strength and electron energy in a CARM are advantageous when compared with competing devices, such as fundamental harmonic gyrotrons and free-electron lasers (FELs). Compared with a gyrotron, the required magnetic field for a CARM device is substantially reduced because of a Doppler frequency upshift of the relativistic cyclotron frequency. Thus, the CARM can provide millimeter and submillimeter radiation in the first electron-cyclotron harmonic using currently available superconducting magnet technology. Compared with a conventional magnetostatic-wiggler FEL, the CARM can reach submillimeter wavelengths at a lower electron-beam voltage. For example, a 500 kV CARM oscillator has the potential for efficient multi-MW operation at wavelengths down to 0.75 mm with a 100 kG superconducting magnet; a 500 kV FEL oscillator with a 3-cm period magnetic-wiggler will produce radiation at ~4.5 mm.[1]

The CARM, like the gyrotron, is a cyclotron maser device, and requires transverse electron momentum to drive the interaction. However, in contrast to the gyrotron, which requires an electron beam with a large momentum pitch ratio $\alpha > 1$ for efficient operation, the CARM can operate efficiently an electron beam with a moderate pitch angle ($\alpha < 0.7$) and a substantial amount of axial momentum. Here $\alpha \equiv p_\perp / p_z$, where $p_\perp$ and p_z are the transverse and parallel components of the electron momentum with respect to the axial magnetic field. The CARM benefits from the Doppler upshift provided by the axial velocity of the beam. The operating frequency of the CARM is given by the simultaneous solution to the two dispersion equations:

$$\omega^2 = \omega_{co}^2 + k^2 c^2 \qquad (1)$$

and

$$\omega = k v_z + \Omega / \gamma \,, \qquad (2)$$

Manuscript approved October 26, 1990.

where (ω,k) are the angular frequency and wave number of the output radiation, ω_{co} is the cutoff frequency of the mode of interest in the cavity, c is the velocity of light, Ω is the nonrelativistic electron cyclotron frequency, and γ is the relativistic factor for the electron beam, defined as $\gamma=\left(1-\beta_z^2-\beta_\perp^2\right)^{-1/2}$, where $\beta_z=v_z/c$, $\beta_\perp=v_\perp/c$, and v_z and $v_\perp$ are the parallel and perpendicular components of the electron velocity with respect to the axial magnetic field. The expression Ω/γ is often referred to as the relativistic cyclotron frequency. The simultaneous solution of the two dispersion equations yields

$$\omega=\gamma_z^2\frac{\Omega}{\gamma}\left\{1\pm\beta_z\left[1-\left(\frac{\omega_{co}}{\gamma_z\Omega/\gamma}\right)^2\right]^{1/2}\right\}, \tag{3}$$

where $\gamma_z=(1-\beta_z^2)^{-1/2}$. This equation will predict the approximate operating frequencies of the cyclotron maser interaction. The upper intersection is the CARM intersection, while the lower intersection corresponds to a gyrotron interaction. For operation at frequencies $\omega>>\omega_{co}$, $\omega\approx 2\gamma_z^2\Omega/\gamma$, an expression similar to that for the upshift of a free-electron laser.

There is fairly extensive literature on the theory and simulation of CARMs and other Doppler-shifted cyclotron maser configurations (see, for example, references 2 and 3) The only experimental CARM oscillator studies reported to date, however, have been the experiments of Botvinnik *et al.*[4], who achieved 6 MW at a wavelength of 4.3 mm and 4% efficiency, and 10 MW at a wavelength of 2.4 mm and 2% efficiency. Preliminary results by Danly and Pendergast[5] have shown significant competition between CARM oscillations and gyrotron oscillations. CARM amplifier results have been reported by Bekefi *et al.*[6].

A CARM oscillator was designed at the Naval Research Laboratory to attain higher efficiency using a higher value of α than that used in previous experiments. Efficiencies greater than 20% are predicted by theory for the design parameters for this oscillator.[3,7] The experimental design parameters are summarized in Table 1.

Beam Voltage	600 kV
Beam Current	200 A
Beam α	0.6
Voltage Pulse Length	50 nsec flat top
Magnetic Field	25 kG
Ω/γ	32 GHz
Operating Mode	TE_{61}
Phase Velocity	1.17c
Power	24 MW
Efficiency	20%

Table 1: NRL 100 GHz CARM oscillator design parameters

II. Experimental details

Figure 1 is a schematic of an experiment designed to produce CARM radiation at 100 GHz in a TE_{61} mode. The annular electron beam is formed by a graphite cathode that is immersed in an axial magnetic field of approximately 10 kG. The electron gun was designed to produce a 200 A annular electron beam with very low initial transverse momentum. The beam then enters a magnetic 'kicker' which imparts some transverse momentum to the beam. Adiabatic compression in the input taper region increases the momentum pitch ratio to $\alpha \sim 0.6$ at a final magnetic field of 23-30 kG. A 10-cm-long region of uniform magnetic field is centered on the Bragg cavity[8, 9]. The cyclotron maser interaction takes place in the cavity, and the beam is subsequently collected on the wall of the output taper.

The voltage for the electron beam was provided by the TRITON accelerator, a Marx generator-Blumlein pulseline accelerator capable of delivering up to 100 kA at 1 MV. Since the experiment operated at currents of less than 1 kA, a radial copper sulfate water resistor was used to shunt most of the current. The shot-to-shot voltage variation was approximately 10%, with >10% rms voltage ripple in the first half of the voltage pulse, and ~5% rms voltage ripple in the second half of the pulse. The electron gun was a graphite field-emission diode with a beam-scraping graphite anode. The electron beam voltage was monitored by a capacitive monitor located on the vacuum vessel wall near the emitter. The net beam current was measured by a self-integrating Rogowski coil just downstream of the beam pump (kicker) magnet. A characteristic voltage trace is shown in Figure 2. The most suitable part of the

voltage pulse for CARM operation is the last 20-30 nsec of the pulse because the voltage ripple decreases throughout the pulse.

The magnetic kicker consists of a localized depression of the axial magnetic field, and is similar to one used by Gold *et al.*[10] in a high voltage gyrotron experiments. If the magnitude of the magnetic field changes on a length scale shorter than a cyclotron orbit, the beam trajectory is not adiabatic, and beam axial momentum can be converted to transverse momentum. A magnetic kicker is simple to construct: a coil is wound on a section of the vacuum vessel, and a current is driven through the coil to produce a field opposite in sense to the main axial field. The combination of a nearly cold beam followed by a magnetic kicker provides a flexible means to create an electron beam suitable for the CARM; the proper choice of operating parameters should generate an electron beam with an α variable between 0.3 and 0.7, and an axial-velocity spread <3%. In this experiment, the beam α and axial velocity spread were not directly measured, but were inferred from computer simulations.

A Bragg cavity was chosen to support the CARM interaction. The cavity is a section of smooth waveguide between two rippled-wall waveguide reflectors[8, 9]. Figure 3 exhibits the design of a Bragg resonator of the type used in this experiment. The Bragg condition for the rippled-wall reflector may be stated as $\lambda_g=2\lambda_r$, where λ_g is the radiation wavelength in the waveguide, and λ_r is the wall ripple period. For a mode and frequency which satisfy the Bragg condition, constructive interference of the small reflections from each of the the ripples can provide a strong total reflection. The Q of the resonator can be increased either by lengthening the uncorrugated section, or by increasing the reflectivity of the corrugated sections. Here, Q is the cavity quality factor.

The calculation of the reflectivity of a corrugated waveguide is a multimode problem involving the coupling coefficients and wavenumber mismatches between the modes. For axisymmetric corrugations, modes can only couple to other modes with the same azimuthal index. When modes of the same azimuthal index have similar cutoff frequencies, the corrugated reflectors must consist of many ripples to avoid coupling between different modes. If the corrugation depth is also sufficiently small to avoid mode conversion effects, then the reflection from the rippled waveguide is

$$R = \tanh^2 GL, \qquad (4)$$

where G is the coupling coefficient for the reflection[9], which is a function of the ripple amplitude and the specific transverse eigenfunction of the mode, and L is the length of

the corrugations. Whispering-gallery (TE_{m1}, $m>>1$) modes couple most strongly to the corrugations, and therefore have the highest reflectivities.

The Q of a reflector consisting of two corrugated sections on either side of an intermediate section of smooth-walled waveguide can be written as

$$Q = \frac{k^2 L_{eff}}{k_z (2 - R_1 - R_2)}, \tag{5}$$

where k is the free-space wavenumber, k_z is the axial wave number, R_1 and R_2 are the reflectivities of the two reflectors, and L_{eff} is the effective length of the cavity. L_{eff} is larger than the length of the intermediate smooth waveguide section because of the energy stored in the rippled-waveguide sections. The parameters for the cavity used are shown in Table 2. The output radiation from the resonator will be a mixture of the TE_{61} and TM_{61} modes due to mode conversion in the output reflector.

Reflector design mode	TE_{61}
Center frequency	100 GHz
Output mode	
TE_{61}	72%
TM_{61}	26%
Upstream reflector length	6.4 cm
Downstream reflector length	4.5 cm
Center section length	4.0 cm
Corrugation period	1.7 mm
Corrugation amplitude	0.12 mm

Table 2. Design parameters of a TE_{61} Bragg Reflector

The microwaves generated in the cavity were transported out of the system in a 5° output taper to a 12.7 cm diameter acrylic window. The V-band (50-75 GHz) and W-band (75-110 GHz) output radiation was measured using a grating spectrometer. The spectrometer has a resolution of approximately 1 GHz and an average insertion loss of 33 dB. The ratio of the area of the spectrometer pick-up to the the area of the output window was ~20. Since the insertion loss was frequency dependent, the spectrometer was separately calibrated at each measured frequency. Three detectors were mounted within the spectrometer, giving the capability of measuring three

different frequencies on each shot. In addition, K_a-band radiation was monitored using a waveguide pickup, a 40 GHz low-pass filter, and a crystal detector.

III. Data.

Microwave measurements were taken for different settings of the electron beam current, and the cathode, cavity, and kicker magnetic fields. For a particular Marx voltage, the beam voltage was determined by the precise timing of the over-voltaged main accelerator switch, and varied ±10% on a shot-to-shot basis. This affected the resonant frequency of the CARM interaction through its effect on the axial electron velocity, v_z , and on the relativistic cyclotron frequency, Ω/γ (see Eq. (3)). By changing the magnetic fields, the frequency at which the electron beam was resonant with a particular waveguide mode (for a specific set of beam parameters) could be varied. In each case, an attempt was made to optimize the interaction by adjusting the level of the kicker magnetic field, which changes v_z as well as the beam α. When a resonance in the Bragg cavity has a sufficiently high Q,and the CARM resonance condition is satisfied at a sufficiently high value of beam α, the CARM should oscillate. For the TE_{61} mode at 100 GHz, the starting current at α=0.6 is predicted to be 40 A.

Figure 4 shows a typical microwave pulse. Microwave pulses generally began ~40-60 nsec into the voltage pulse. At each shot in which high frequency ($f \sim 100$ GHz) radiation was produced, lower frequency microwaves ($f \sim 35$ GHz) attributed to the gyrotron interaction were also observed. The maximum power coupled into the spectrometer (not corrected for the area of the pickup) was ~500 watts in a single channel, giving an estimated total power output of ~10 kW per 1 GHz channel. Power was estimated by correcting the power measured by a spectrometer diode for the insertion loss of the spectrometer and multiplying by the ratio of the area of the output window to the area of the spectrometer pick-up. Since the overall powers were significantly lower than those anticipated in the experimental design, no attempt was made to obtain accurate total power measurements. The frequencies that corresponded to the expected TE_{m1} Bragg modes showed no more power than other portions of the microwave spectrum. The TE_{61} mode is expected to resonate at 100 GHz, the TE_{51} mode should oscillate at 97 GHz, and the TE_{71} mode should occur at 103 GHz.[9]

The current required to produce microwaves was higher than the predicted cold-beam start current for the CARM oscillator. This suggests that the electron beam had greater spread than that predicted by the electron trajectory codes, possibly

due to a lower beam quality than predicted by our numerical simulations. It is also possible that due to machining tolerances, the Q of the Bragg resonator was lower than its design value. (Efforts to cold test the TE_{61} Bragg mode of the resonator were unsuccessful, due to the inability to launch this mode into the resonator.)

Figure 5 shows the spectrum of microwave emission from the experiment for a series of shots. Each bar is an average of many shots. The striped bars represent data taken with the rippled-wall cavity, while the solid bars represent data with a smooth circular waveguide installed in place of the cavity. The gaps in the spectrum don't indicate an absence of microwaves; these gaps are frequencies where no measurements were taken. Clearly, the resonator has little effect on the spectrum of the microwaves. Furthermore, microwaves were observed at all frequencies in the spectrometer where detectors were placed, with no large power difference between different frequencies. The only observed effect of the Bragg resonator was the occurrence of microwave radiation approximately 10 nsec earlier in the voltage pulse than with a smooth walled waveguide. Since the feedback provided by the high-Q Bragg resonator would be required for the CARM mode to oscillate, we conclude that no radiation attributable to a CARM interaction was observed.

The absence of CARM radiation is probably due to competition with gyrotron and gyro-BWO modes both in the fundamental and in the second and third harmonics. Figure 6 shows the uncoupled beam-waveguide dispersion relation for a waveguide of the same diameter as our Bragg cavity, and indicates the richness of the mode spectrum in the frequency range of the desired CARM operating interaction. In order to reduce the clutter of modes in the figure, only the modes expected to couple most strongly with the electron beam (TE_{m1} and TE_{m2}) are shown. The TE_{61} mode is depicted with a thick line. Also shown are the electron beam lines for the first three cyclotron harmonics. Harmonic gyrotron oscillations occur where the electron beam lines intersect the waveguide dispersion relation near $k_z = 0$. If the electron beam line intersects the waveguide dispersion with $k_z < 0$, the interaction is a gyro-backward-wave interaction. Since backward-wave oscillations are absolutely unstable, they need no external feedback structure, and will oscillate in a smooth-walled waveguide as well as in the Bragg cavity.

Most of the high-frequency radiation from the experiment is attributed to third-harmonic backward-wave oscillations; the remainder of the modes could be either CARM modes or gyrotron modes. As seen in Figure 6, the third harmonic of the beam cyclotron mode can interact with many backward waves of the waveguide system and generate radiation in the same frequency band as that predicted for CARM radiation. Using the results of Davies[11], we have calculated the growth rates and frequencies of

the backward-wave oscillations. In order to compare the microwave data with this theory, we have estimated the growth rates of the microwave signals by using the measured time interval between the beginning of the flat portion of the voltage pulse and the emergence of the microwave pulses on the oscilloscope traces. Figure 7 shows the calculated growth rate of the backward-wave interactions along with the measured growth rates of the microwave signals. The solid line is the growth rate for the backward waves with the strongest coupling to the electron beam. The hollow diamonds represent the growth rates of the microwaves measured in the smooth-walled waveguide. The crosses represent the growth rates of the microwaves measured in the Bragg cavity. The form of the frequency dependence of the growth rate shows agreement between theory and data. Microwaves generated with the Bragg cavity installed appear to rise somewhat more quickly than those in the smooth-walled waveguide, indicating that the ripples may provide some additional feedback for the backward-wave interaction.

The calculated growth rates of the absolute instabilities are comparable to those predicted for the whispering-gallery CARM modes. The backward-wave spectrum is sufficiently dense that mode discrimination is not possible with our experimental setup. A lack of shot-to-shot reproducibility prevented identification of specific modes.

IV. Summary

We have carried out a CARM oscillator experiment designed to produce tens of MWs of 100 GHz radiation from an interaction between a 600 keV, 200 A, α~0.6 annular electron beam and an axial magnetic field of 23-30 kG. The experiment employed a Bragg resonator designed to operate in the TE_{61} mode. The electron beam was produced by a pulseline accelerator using a field-emission cathode. The experiment produced moderate amounts of radiation (tens of kW per 1-GHz wide channel) at nearly all frequencies in the 70-100 GHz range. Most of this radiation is attributed to the harmonic gyro-backward-wave oscillation mechanism, however, because the frequencies fall in ranges midway between gyrotron harmonic frequencies, and at frequencies where the Bragg resonator will not work. Some of the radiation could be CARM or harmonic gyrotron, but no clearly discernable CARM radiation was observed. In addition, every set of operating parameters that produced high-frequency radiation also produced radiation in the vicinity of 35 GHz that is attributed to a first harmonic gyrotron interaction. The lack of observable CARM radiation is attributed to mode competition, due in part to poor voltage regulation in the accelerator. Since the CARM needs $\Delta v_z/v_z < 4\%$ to grow effectively, the portion of the voltage pulse suitable

for CARM operation is limited to 20-30 nsec near the end of the voltage pulse, after competing third-harmonic gyrotron and gyro-backward-wave oscillations have already had a chance to grow.

This study points out the difficulty of producing CARM radiation in highly overmoded waveguides with high power or efficiency because of competition with backward-wave modes. Since these non-CARM modes have small parallel wave vectors, it may be possible to increase the start currents of these competing modes by selective slotting and loading of the resonator walls. For instance, alternating rings of conducting and lossy materials may be effective in discriminating between modes with long wavelengths and the CARM modes with short wavelengths. Most likely, however, the problem of backward-wave instabilities in CARMs will persist as long as waveguide structures are used to support the interaction.

V. Acknowledgment

This work was supported by the Office of Naval Research.

VII. References

[1] V. L. Granatstein, 1988, *Proc. of the 1987 Particle Accelerator Conf.*, (Washington, D. C. IEEE)

[2] A. T. Lin and C. C. Lin, "Doppler shift dominated cyclotron maser amplifiers," *Int. J. Infrared Millimeter Waves,* Vol. **6**, pp. 41-51, 1985.

[3] A. W. Fliflet, "Linear and non-linear theory of the Doppler-shifted cyclotron resonance maser based on TE and TM waveguide modes," *Int. J. Electron.,* Vol. **61**, no. 6, pp. 1049-1080, June, 1986.

[4] I. E. Botvinnik, V. L. Bratman, A. B. Volkov, G. G Denisov, B. D. Kol'chugin, and M. M. Ofitserov, "Cyclotron-autoresonance maser with a wavelength of 2.4 mm," *Pis'ma Zh. Tekh. Fiz.,* Vol. **8**, pp. 1386-1389, 1982; also *Sov. Tech. Phys. Lett.,* Vol **8**, pp 596-597.

[5] B. G. Danly, Private communication, August, 1990 .

[6] G. Bekefi, A. C. DiRienzo, C. Leibovitch, and B. G. Danly, "35 GHz cyclotron autoresonance maser amplifier," *Appl. Phys. Lett.,* Vol. **54**, pp. 1302-1304, April 3, 1989.

[7] R. B. McCowan, A. W. Fliflet, S. H. Gold, W. M. Black, A. K. Kinkead, V. L. Granatstein, and M. Sucy, "Design of a 100 GHz CARM oscillator experiment," *IEEE Trans. Electron Devices,* Vol. **36**, no. 9, pp. 1968-1975, September, 1989.

[8] V. L. Bratman, G. G. Denisov, N. S. Ginzburg, and M. I. Petelin, "FEL's with Bragg Reflection Resonators: Cyclotron Autoresonance Masers Versus Ubitrons," *IEEE J. Quantum Electron.,* Vol. **QE-19**, no. 3, pp. 282-296, March, 1983.

[9] R. B. McCowan, A. W. Fliflet, S. H. Gold, V. L. Granatstein, and M. C. Wang, " Design of a waveguide resonator with rippled-wall reflectors for a 100 GHz CARM oscillator experiment.," *Int. J. Electron.,* Vol. **65**, no. 3, pp. 463-475, 1988.

[10] S. H. Gold, A. W. Fliflet, W. M. Manheimer, R. B. McCowan, W. M. Black, R. C. Lee, and V. L. Granatstein, "High peak power Ka-band gyrotron oscillator experiment," *Phys. Fluids,* Vol. **30**, no. 7, pp. 2226-2238, 1987.

[11] J. A. Davies, "Conditions for absolute instability in the cyclotron resonance maser," *Phys. Fluids B,* Vol. **1**, no. No 3, pp. 663-669, March, 1989.

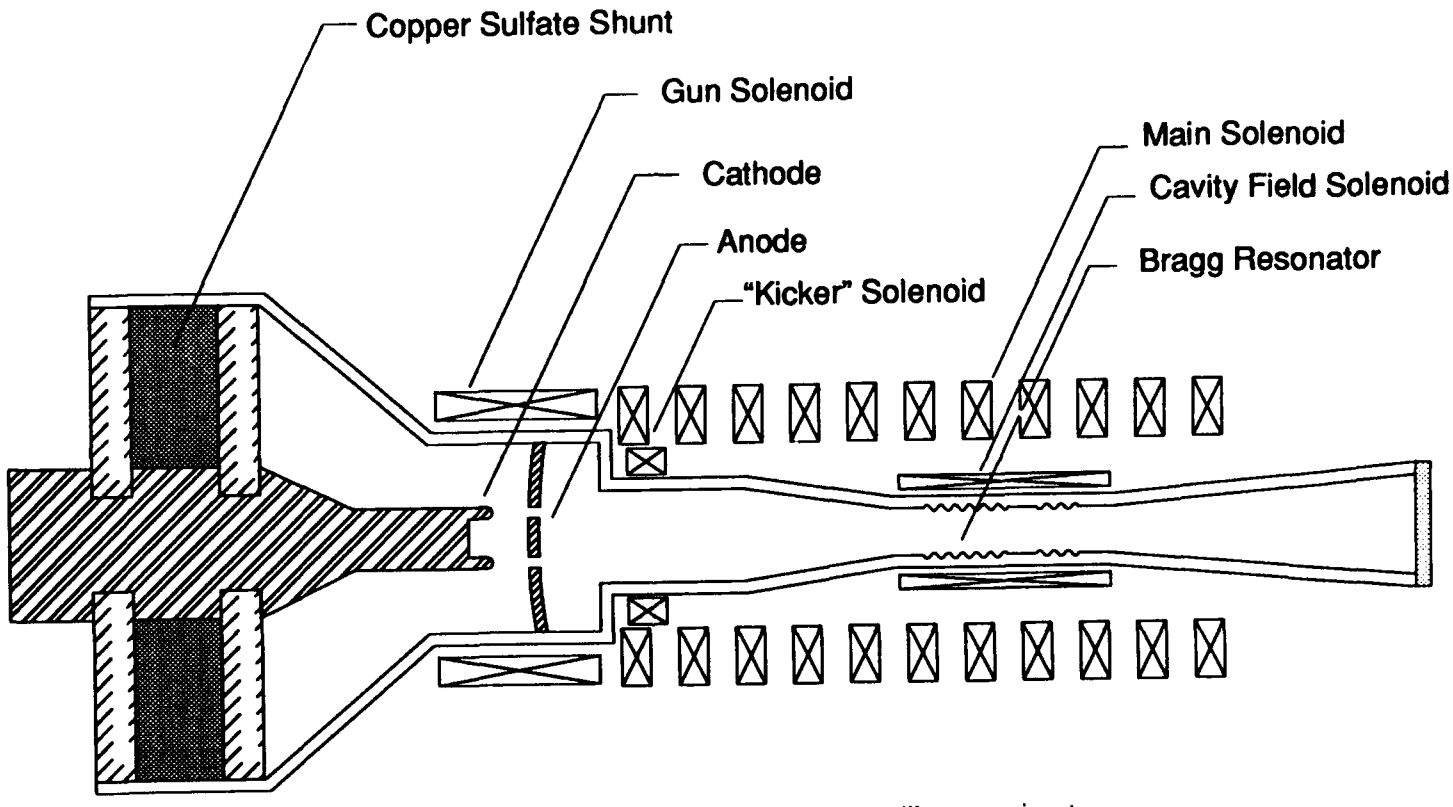

Fig. 1 — Diagram of the NRL CARM oscillator experiment

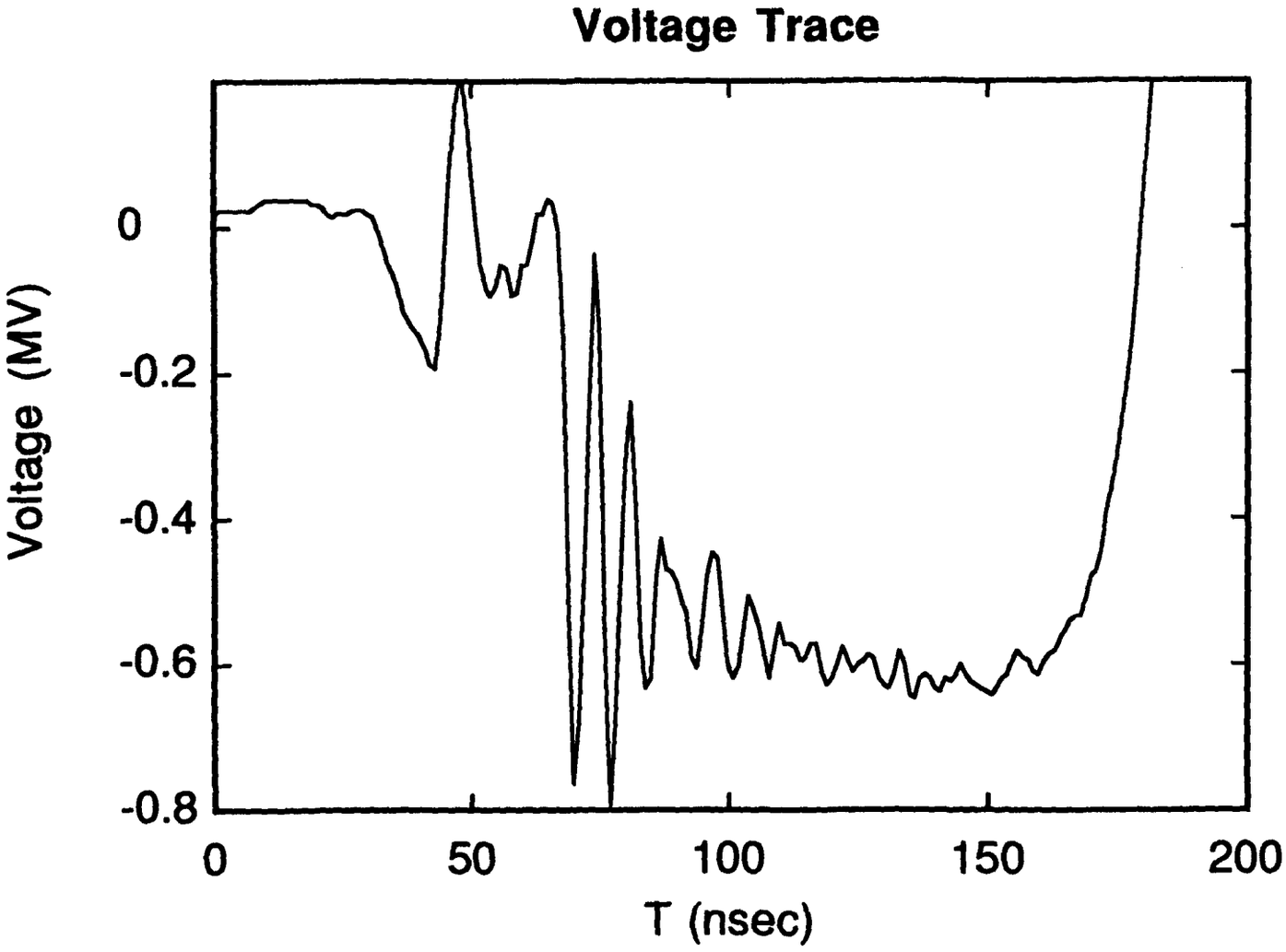

Fig. 2 — A typical voltage trace from the accelerator used in the CARM experiment

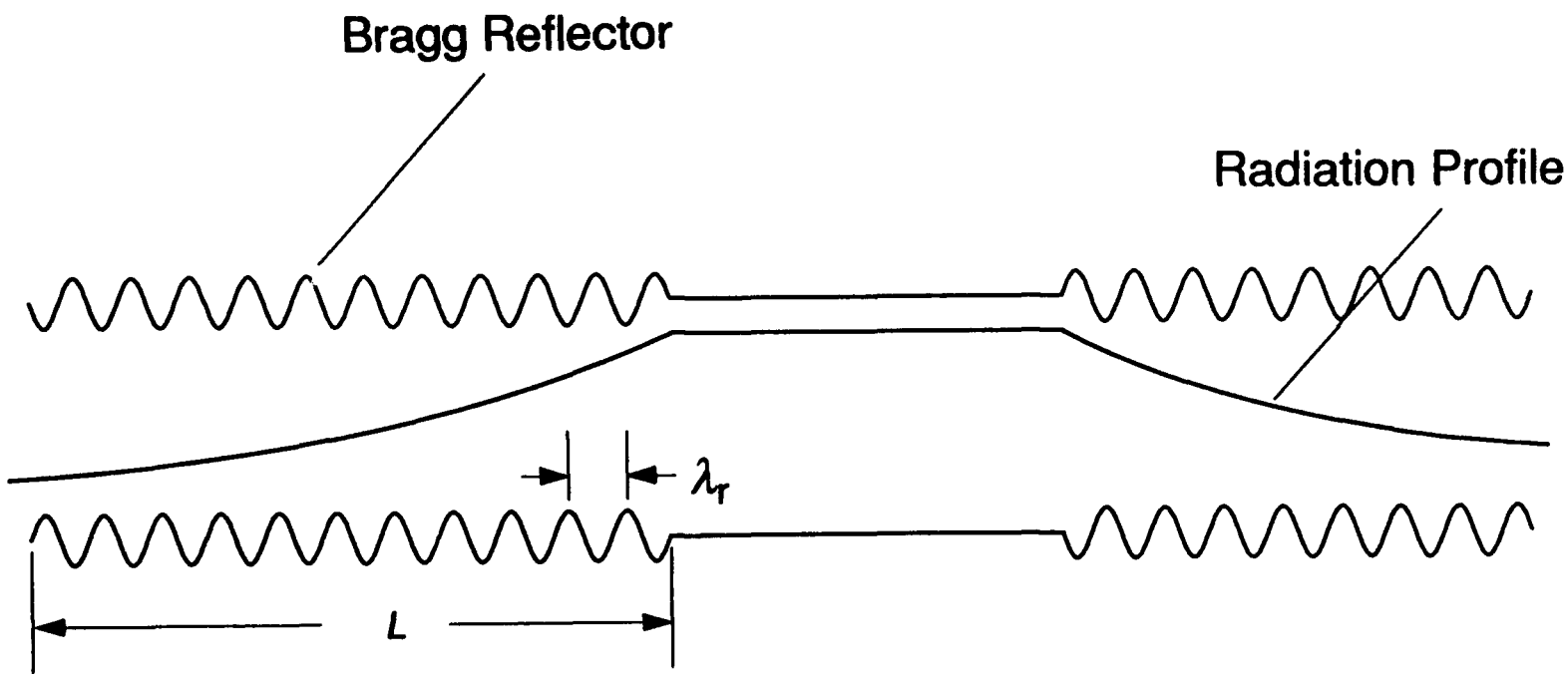

Fig. 3 — A diagram of the Bragg resonator

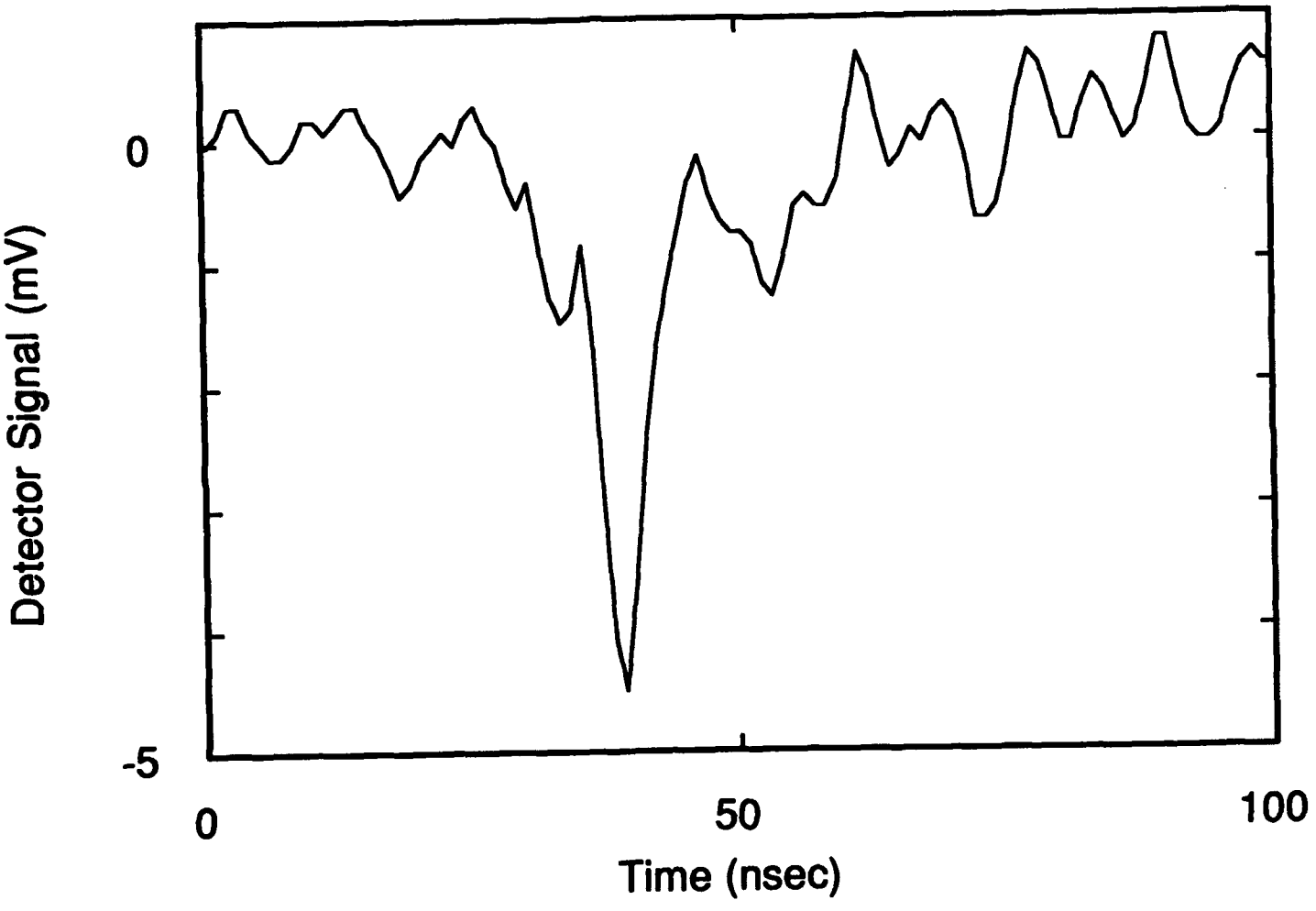

Fig. 4 — A typical microwave pulse from the experiment

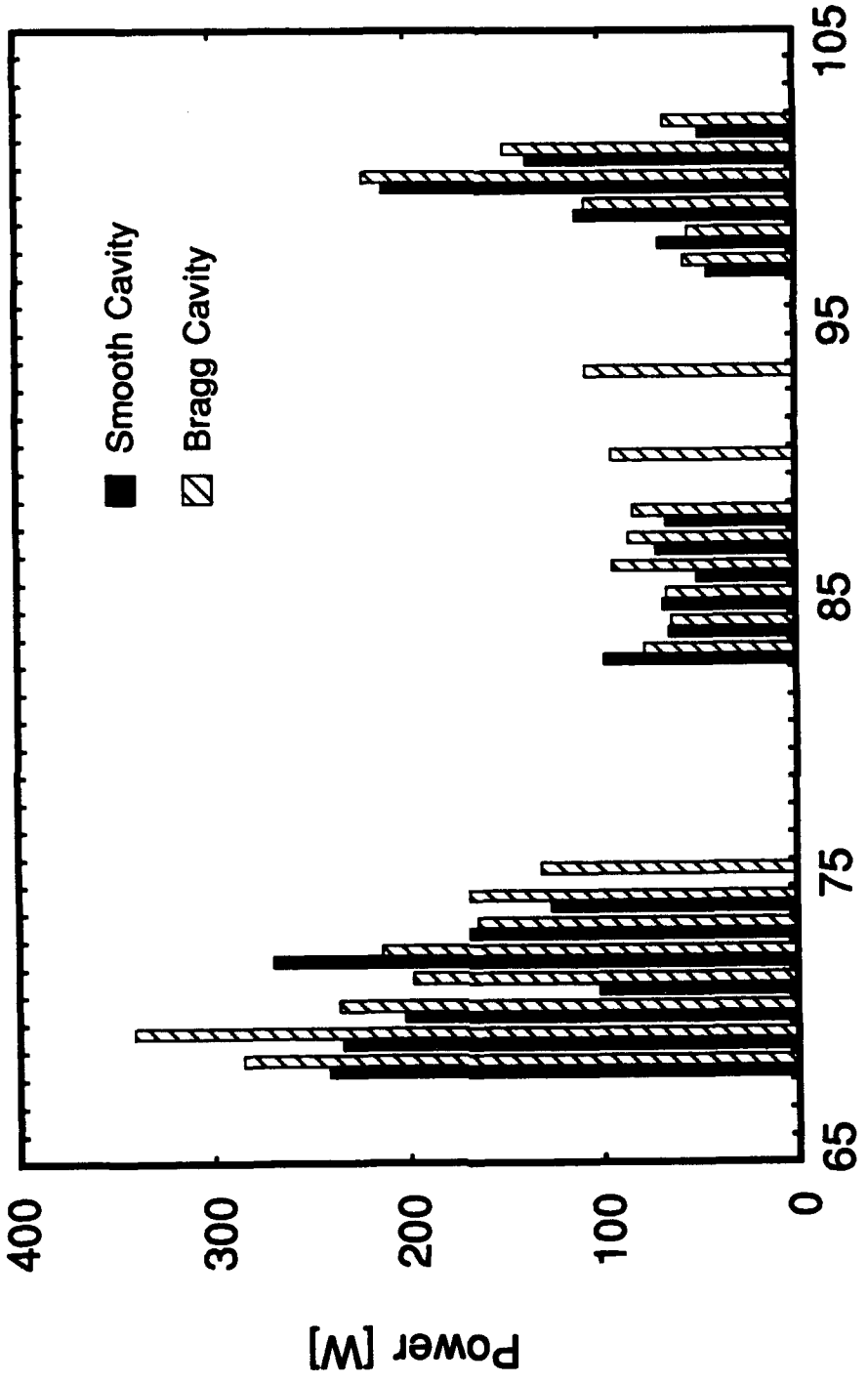

Fig. 5 — The spectrum with and without Bragg resonator

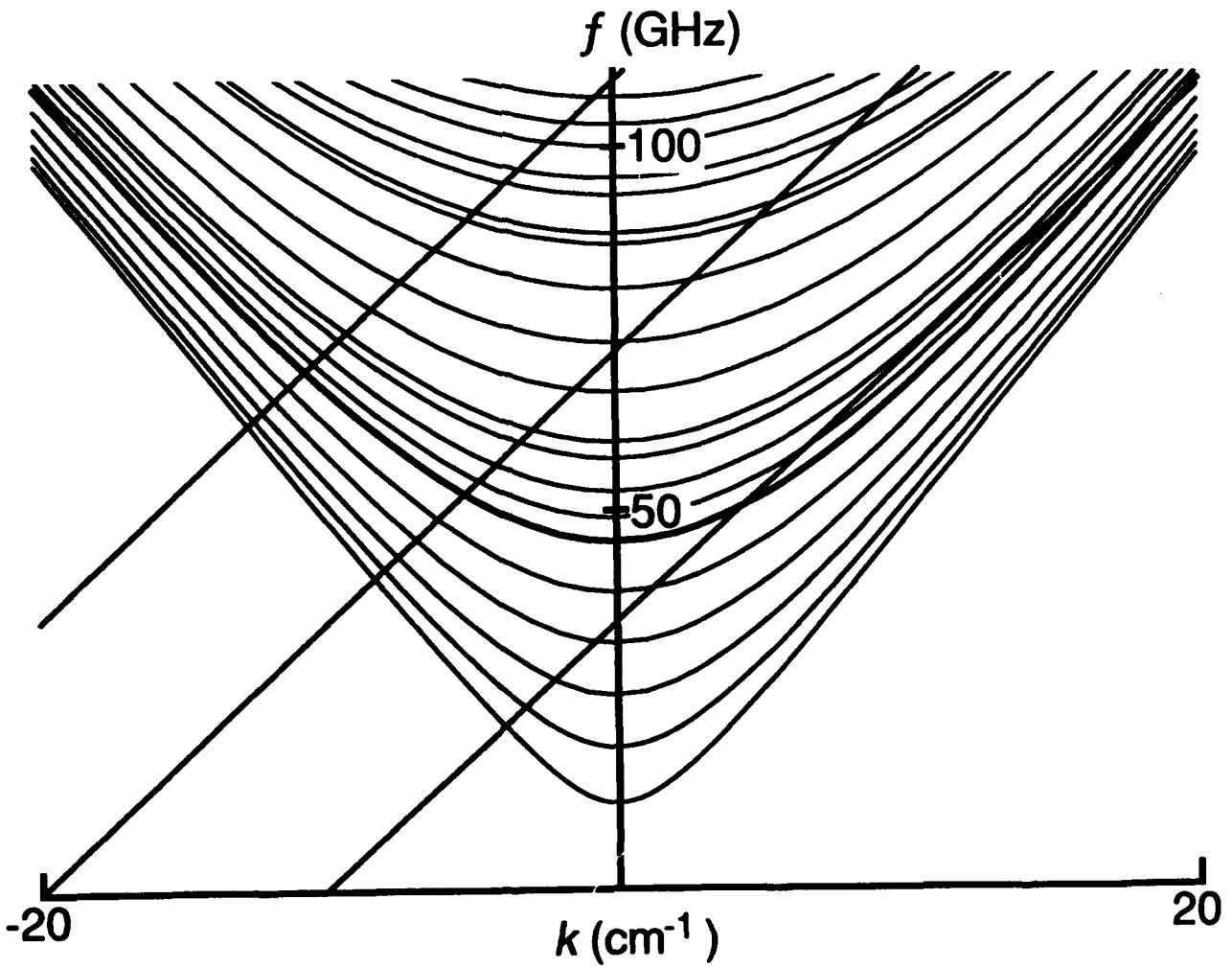

Fig. 6 — The uncoupled beam-dispersion relation including harmonics

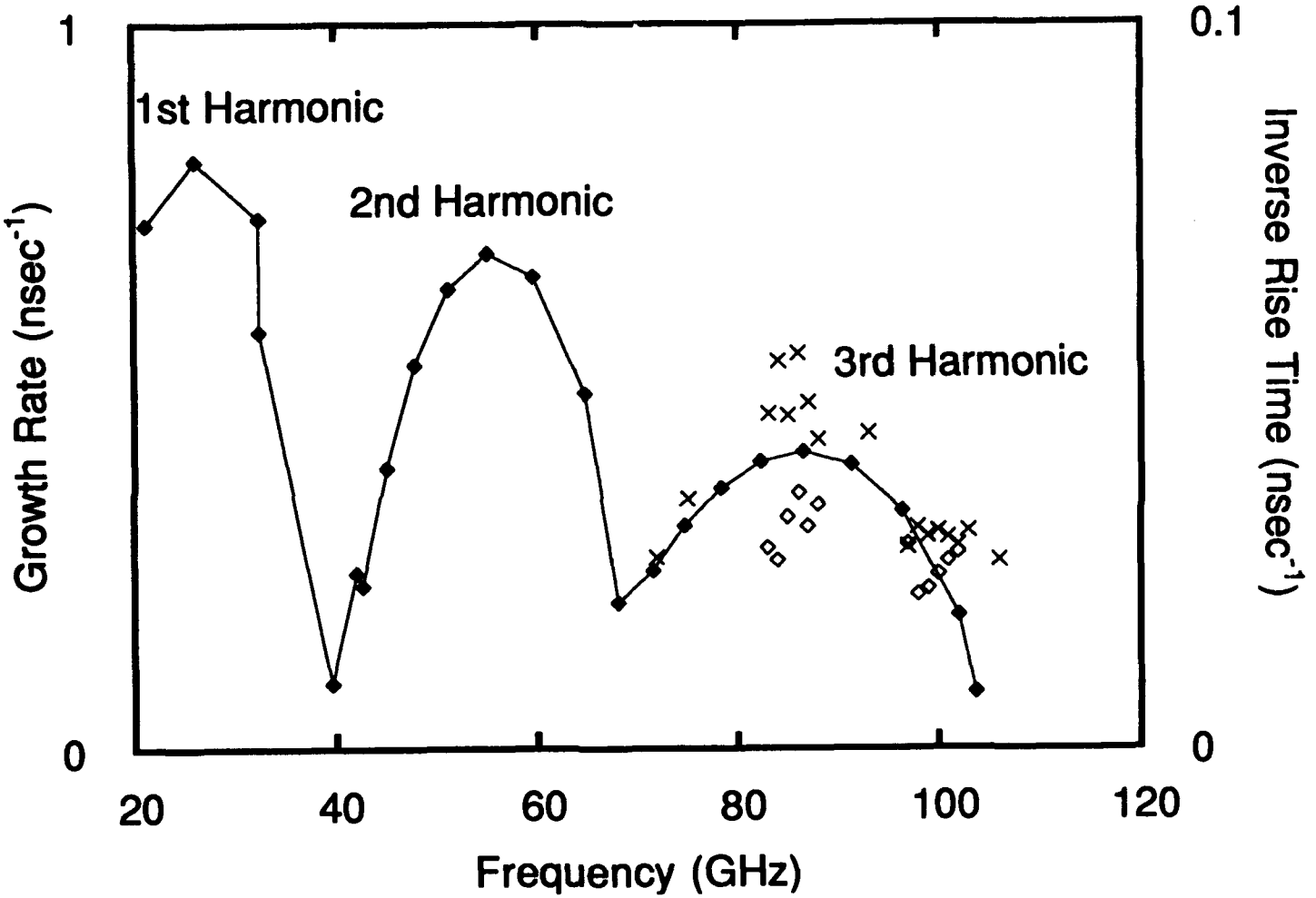

Fig. 7 — The growth rates of the backward wave instabilities. Solid diamonds are theoretical values and correspond to the left-hand axis. The crosses are measurements with the Bragg resonator installed, while the hallow diamonds are measurements with the smooth-wall circular waveguide installed. The experimental points correspond to the right-hand axis